Cell Metabolism
Article

Deletion of Iron Regulatory Protein 1 Causes Polycythemia and Pulmonary Hypertension in Mice through Translational Derepression of HIF2α

Manik C. Ghosh,[1,6] De-Liang Zhang,[1,6] Suh Young Jeong,[1] Gennadiy Kovtunovych,[1] Hayden Ollivierre-Wilson,[1] Audrey Noguchi,[2] Tiffany Tu,[1] Thomas Senecal,[1] Gabrielle Robinson,[1] Daniel R. Crooks,[1] Wing-Hang Tong,[1] Kavitha Ramaswamy,[1] Anamika Singh,[1] Brian B. Graham,[3] Rubin M. Tuder,[3] Zu-Xi Yu,[2] Michael Eckhaus,[4] Jaekwon Lee,[5] Danielle A. Springer,[2] and Tracey A. Rouault[1,*]

[1]Molecular Medicine Program, Eunice Kennedy Shriver National Institute of Child Health and Human Development, Bethesda, MD 20892, USA
[2]Murine Phenotyping Core, National Heart, Lung, and Blood Institute, Bethesda, MD 20892, USA
[3]Program in Translational Lung Research, Division of Pulmonary Sciences and Critical Care Medicine, Department of Medicine, University of Colorado School of Medicine, Denver, CO 80262, USA
[4]Veterinary Resources Program, National Institutes of Health, Bethesda, MD 20892, USA
[5]Department of Biochemistry, University of Nebraska-Lincoln, NE 68588, USA
[6]These authors contributed equally to this work
*Correspondence: rouault@mail.nih.gov
http://dx.doi.org/10.1016/j.cmet.2012.12.016

SUMMARY

Iron regulatory proteins (Irps) 1 and 2 posttranscriptionally control the expression of transcripts that contain iron-responsive element (IRE) sequences, including ferritin, ferroportin, transferrin receptor, and hypoxia-inducible factor 2α (HIF2α). We report here that mice with targeted deletion of *Irp1* developed pulmonary hypertension and polycythemia that was exacerbated by a low-iron diet. Hematocrits increased to 65% in iron-starved mice, and many polycythemic mice died of abdominal hemorrhages. *Irp1* deletion enhanced HIF2α protein expression in kidneys of *Irp1*$^{-/-}$ mice, which led to increased erythropoietin (EPO) expression, polycythemia, and concomitant tissue iron deficiency. Increased HIF2α expression in pulmonary endothelial cells induced high expression of endothelin-1, likely contributing to the pulmonary hypertension of *Irp1*$^{-/-}$ mice. Our results reveal why anemia is an early physiological consequence of iron deficiency, highlight the physiological significance of Irp1 in regulating erythropoiesis and iron distribution, and provide important insights into the molecular pathogenesis of pulmonary hypertension.

INTRODUCTION

Iron is an essential element to virtually all organisms, as it is a crucial component of heme and iron sulfur proteins and is indispensable for DNA replication, oxygen transport, and ATP production. Iron deficiency usually causes anemia, whereas iron overload can generate reactive oxygen species and damage lipids, DNA, and proteins in diseases such as hemochromatosis, cancer, and cardiovascular and neurodegenerative diseases (reviewed in Rouault, 2006; Hentze et al., 2010). Therefore iron homeostasis must be precisely regulated.

Cellular iron homeostasis is mainly controlled by the iron-regulatory protein (Irp)/iron-responsive element (IRE) machinery in mammalian cells. Iron-regulatory proteins regulate the expression of target proteins posttranscriptionally by binding to IREs in transcripts that mostly encode iron metabolism proteins, including the iron storage proteins, H- and L-ferritin, iron uptake proteins, transferrin receptor 1 (Tfrc), divalent metal transporter 1 (Dmt1), the iron export protein, ferroportin, and several other transcripts. By inhibiting the translation of proteins involved in iron export, storage, and utilization, and stabilizing the transcripts of proteins involved in iron uptake, the Irp/IRE machinery regulates cellular iron homeostasis in response to intracellular iron status (Rouault, 2006; Hentze et al., 2010). Though the two Irps, Irp1 and Irp2, share high sequence similarity, they are regulated by different mechanisms. Irp1 is a bifunctional protein that binds to IREs in iron-deficient conditions when it is an apoprotein, but it converts to cytosolic aconitase in iron-replete conditions upon acquisition of a [4Fe-4S] cluster in the active site cleft that separates domains 1–3 from domain 4 (Dupuy et al., 2006; Walden et al., 2006). Irp2 is active as an IRE-binding protein in iron-deficient cells, because it is otherwise rapidly degraded in iron-replete conditions as a result of FBXL5-mediated ubiquitination and subsequent proteasomal degradation (Salahudeen et al., 2009; Vashisht et al., 2009). Previously, we and others reported that mice with a targeted deletion of *Irp2* (*Irp2*$^{-/-}$) developed adult-onset neurodegeneration and anemia (LaVaute et al., 2001; Cooperman et al., 2005; Galy et al., 2005), as the tissues and cells that were adversely affected were largely dependent on Irp2 for regulation, and residual Irp1 did not appear to compensate for the loss of Irp2 in affected cells, whereas Irp2 could compensate for loss of Irp1 in many cells (Meyron-Holtz et al., 2004a). Complete loss of Irp1 and Irp2 causes early embryonic lethality, implying that Irp1 and Irp2 have redundant functions (Smith et al., 2006). However, mice with a targeted deletion of

Irp1 (*Irp1*$^{-/-}$ mice) did not display an easily recognizable phenotype when maintained on a normal iron diet, which raised questions about the physiological role of Irp1 in iron homeostasis.

One of the more recently identified targets of the Irp/IRE system is HIF2α (also known as Endothelial PAS Domain protein 1, EPAS1), a transcription factor that belongs to the hypoxia-inducible factor (HIF) α protein family. In response to hypoxia, anemia, or iron deficiency, HIF2α heterodimerizes with HIF1β and translocates into the nucleus to regulate the expression of genes involved in the adaptive response to hypoxia, including erythropoietin (EPO) (Semenza, 2012). Under normoxia, prolyl hydroxylase domain protein 2 (PHD2) site-specifically hydroxylates HIF2α, thereby targeting the latter for ubiquitination by the von Hippel-Lindau (vHL) E3 ligase complex and proteasomal degradation (Kaelin and Ratcliffe, 2008). Evidence is growing that HIF2α is the master regulator for erythropoiesis in the adaptive response to hypoxia, and mutations of the proteins in this pathway, including HIF2α, PHD2, and vHL, are implicated in dysregulation of erythropoiesis (Majmundar et al., 2010). Recently it was found that HIF2α contains an IRE in its 5′UTR, and Irps could bind and inhibit the translation of HIF2α mRNA in vitro, suggesting that iron homeostasis and erythropoiesis could be potentially linked by HIF2α (Sanchez et al., 2007; Zimmer et al., 2008). However, the relevance of the IRE in the 5′UTR of the HIF2α transcript in mammalian physiology has not been established.

In this study, to investigate the physiological significance of Irp1 in iron metabolism, we challenged *Irp1*$^{-/-}$ mice with iron deficiency, and we found that deletion of *Irp1* increased HIF2α expression, which in turn stimulated EPO and endothelin-1 expression, leading to polycythemia, pulmonary hypertension, and early sudden death from hemorrhage.

RESULTS

Irp1$^{-/-}$ Mice on Low-Iron Diet Die Early of Abdominal Hemorrhages

To challenge the mice with iron deficiency, we maintained the wild-type (WT) and *Irp1*$^{-/-}$ mice (15–18 per group) on a low-iron diet for up to 24 months. We found that the *Irp1*$^{-/-}$ mice on the low-iron diet were prone to sudden death when they were as young as 3 months of age (Figure 1A, see Figure S1A online), and 50% of these mice had died by the age of 10 months. The autopsies revealed gross abdominal hemorrhages as the presumed cause of death for almost all of the *Irp1*$^{-/-}$ mice that died while on the low-iron diet (Figure 1B). To further characterize the causes of sudden death, we evaluated the iron status and tissue pathology of *Irp1*$^{-/-}$ mice. Compared with their WT counterparts, *Irp1*$^{-/-}$ mice had low serum iron levels (Figure 1C), lower transferrin saturations (Figure 1D), and low stainable nonheme iron in tissues such as spleen and bone marrow (Figure 1E, Figure S1B), suggestive of systemic iron deficiency. However, low dietary iron uptake was not the cause of iron deficiency in *Irp1*$^{-/-}$ mice, as the intestinal iron uptake machinery was functional and responsive (Figures S1C–S1E).

Irp1$^{-/-}$ Mice Develop Polycythemia with Extramedullary Erythropoiesis

To determine whether abnormal erythropoiesis was responsible for the abdominal hemorrhages that caused early death, we evaluated complete blood counts of *Irp1*$^{-/-}$ mice. Strikingly, hematocrits of *Irp1*$^{-/-}$ animals were elevated on the normal diet and increased further, to as high as 65% in *Irp1*$^{-/-}$ mice, on the low-iron diet (Figure 2A). The hematocrits were also increased in young *Irp1*$^{-/-}$ animals (Figure S2A). RBC and hemoglobin levels were higher in *Irp1*$^{-/-}$ mice, whereas MCV and MCH levels were lower, consistent with systemic iron deficiency in *Irp1*$^{-/-}$ mice (Table S1). Extramedullary erythropoiesis increased in *Irp1*$^{-/-}$ mice, especially in the mice maintained on a low-iron diet, as evidenced by expansion of splenic red pulp (Figure 2B), gross splenomegaly (Figure 2C, Figure S2B), and increased percentages of Ter119-positive immature erythroid cells as assessed by fluorescence-activated cell sorting (FACS) analysis (Figure 2D). We did not see evidence for an expansion of hematopoiesis in bone marrow cross-sections of *Irp1*$^{-/-}$ mice (Figure S2D). Though the spleen showed less ferric nonheme iron in histologic stains (Figure 1E), total splenic iron measured by ICP-MS was higher in *Irp1*$^{-/-}$ mice on the normal diet (Figure S2C), suggesting that splenic iron was mainly incorporated into heme. Thus, increased diversion of iron for expanded erythropoiesis likely caused systemic iron deficiency, as evidenced by low serum transferrin saturations and low tissue iron stains (Figures 1C–1E).

To determine the cause of polycythemia in *Irp1*$^{-/-}$ mice, we analyzed levels of EPO and observed that both serum EPO (Figure 2E) and EPO mRNA levels in kidney (Figure S2E) were significantly increased in *Irp1*$^{-/-}$ mice, especially in mice on the low-iron diet. Because EPO is a known transcriptional target of HIF2α (Semenza, 2012), we assessed the HIF2α protein levels in renal lysates of WT and *Irp1*$^{-/-}$ animals (Figure 2F) and observed that HIF2α protein levels were increased in the EPO-producing interstitial renal fibroblasts (Pan et al., 2011) of *Irp1*$^{-/-}$ mice, particularly in the mice on low-iron diet (Figure 2G, Figure S2F). Since the HIF2α transcript is a known Irp1 target (Sanchez et al., 2007; Zimmer et al., 2008), and HIF2α mRNA levels remained unchanged (Figure S2G), we hypothesized that loss of Irp1 allowed unrepressed translation of HIF2α in interstitial fibroblasts, which activated expression of HIF2α target genes including EPO, and thereby increased red blood cell (RBC) production, causing polycythemia (Figure 2A) and redistribution of iron from tissues to developing erythroid cells (Figure 1E).

Irp1$^{-/-}$ Mice Develop Pulmonary Hypertension

Since high hematocrits stress cardiovascular function, we evaluated the potential contribution of cardiac disease to the phenotype of sudden death with cardiac ultrasound. Abnormal motion of the interventricular wall during systole in *Irp1*$^{-/-}$ animals suggested that there was pulmonary hypertension (Figure 3A, Movie S1). There was also hypertrophy of the cardiac walls (Figures 3B and 3C). Systolic ejection fractions did not change in *Irp1*$^{-/-}$ mice, indicating normal cardiac contractility (Figure S3A). Catheterization of the right ventricle revealed that pulmonary pressures were significantly elevated in *Irp1*$^{-/-}$ animals at both 3 and 12 months of age (Figure 3D) but did not increase further in *Irp1*$^{-/-}$ mice on low-iron diet, in contrast to the polycythemic response. At autopsy, areas of fibrosis and cardiomyocyte degeneration were present throughout the heart (Figure 3E, Figure S3E). However, discernible changes in the pulmonary vasculature (Figures S3B and S3C) and thromboses were rarely

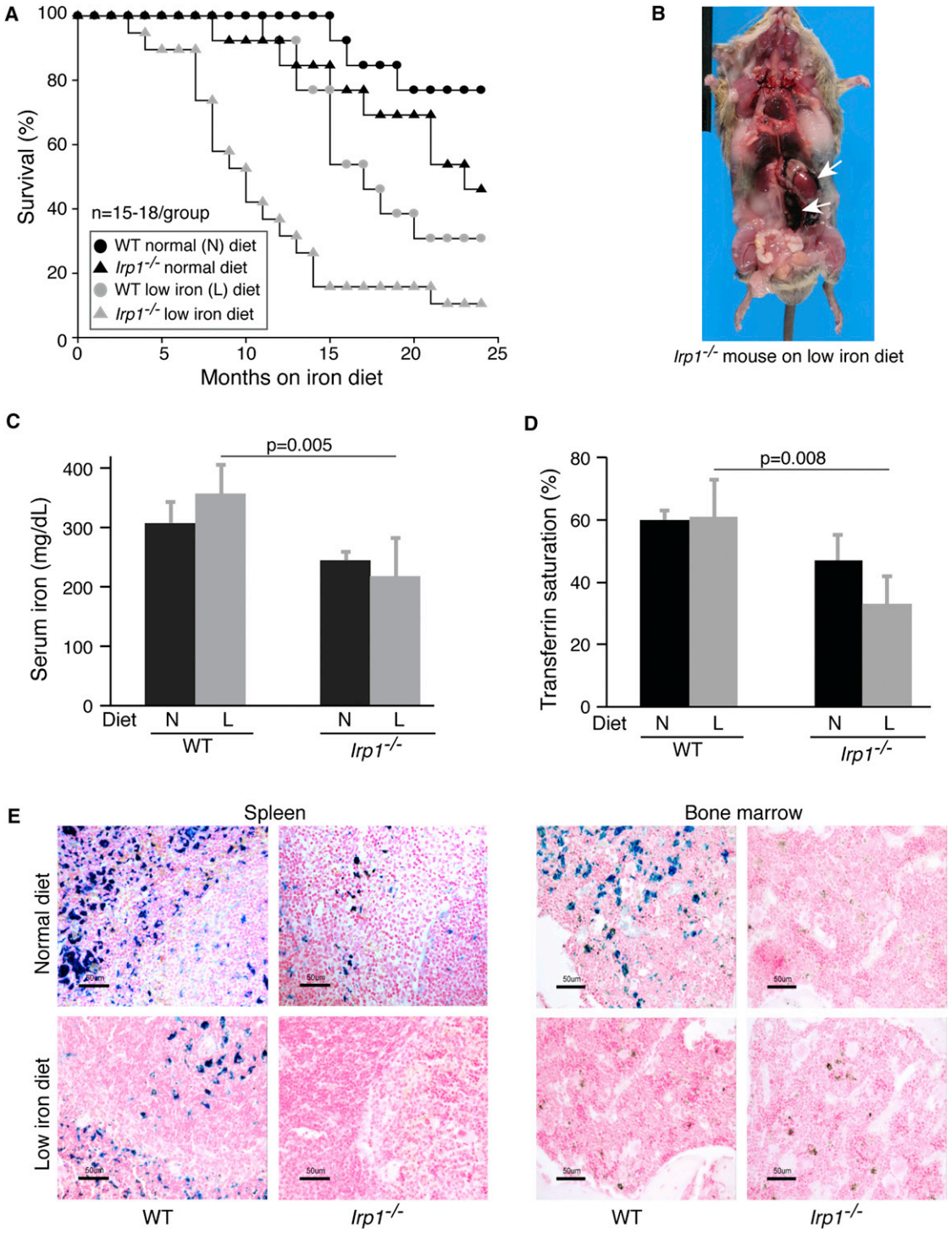

Figure 1. Reduced Life Expectancy of *Irp1*$^{-/-}$ Mice Is Exacerbated by Iron Deficiency

(A) Survival curves for mice with indicated genotypes and diets.

(B) Image of a 3-month-old low-iron-diet *Irp1*$^{-/-}$ mouse that died from abdominal hemorrhage in the perinephric area (white arrows).

(C and D) (C) Serum iron and (D) transferrin saturation in 1-year-old normal diet (N) or low-iron diet (L) mice (n = 5 per group) showing iron deficiency in low-iron-diet *Irp1*$^{-/-}$ mice.

(E) Representative Prussian blue staining of spleen and bone marrow of WT and *Irp1*$^{-/-}$ mice maintained on normal (N) or low-iron (L) diets showing low ferric nonheme iron stores in *Irp1*$^{-/-}$ mice (n = 4–5 per group). Data are represented as mean ± SD. See also Figure S1.

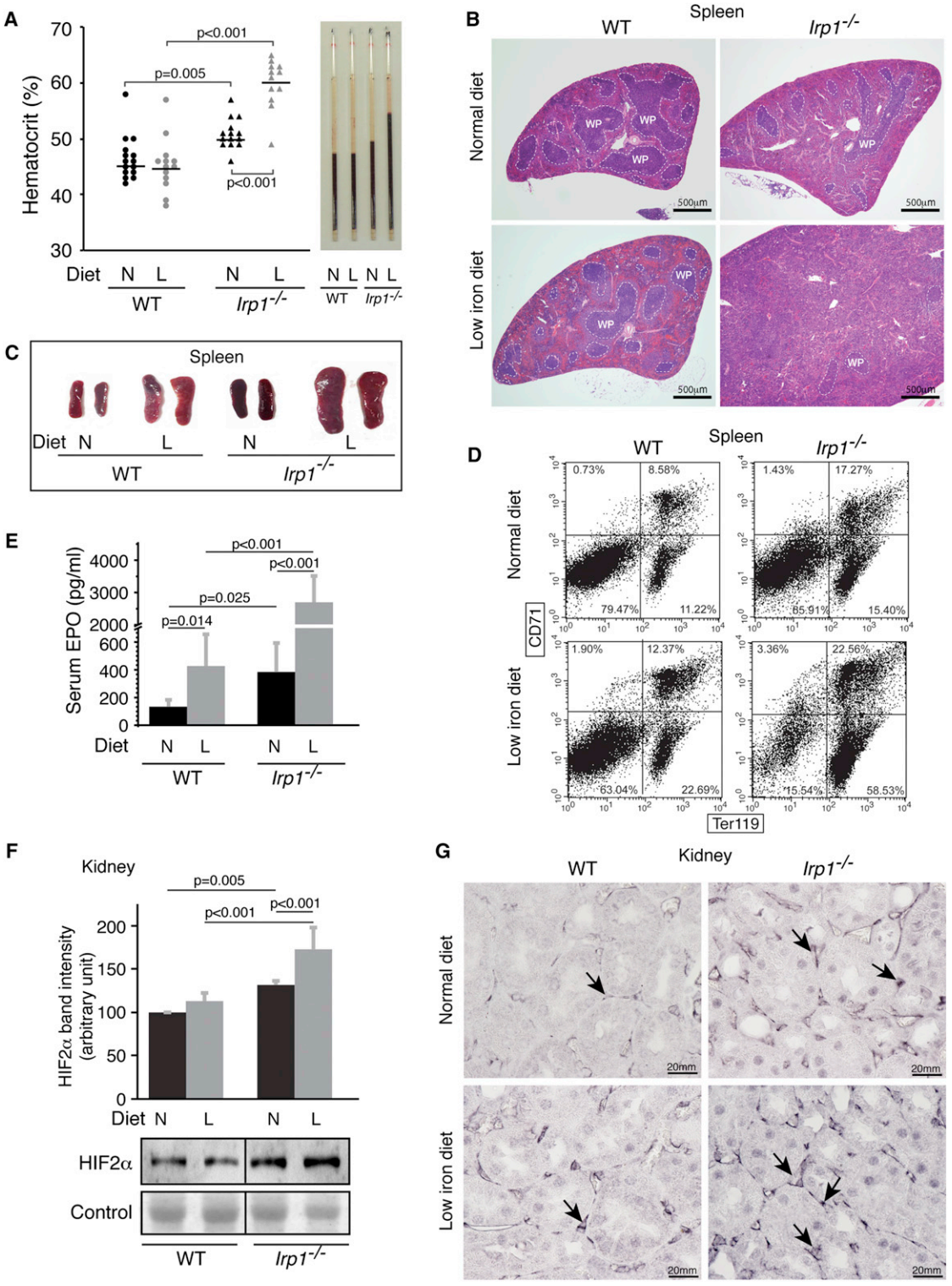

Figure 2. *Irp1*$^{-/-}$ Mice Have Polycythemia and Enhanced Extramedullary Hematopoiesis, High Serum EPO, and Elevated Renal HIF2α Expression

(A) Hematocrits of 1-year-old animals as determined by capillary tube centrifugation were significantly higher in *Irp1*$^{-/-}$ mice on both normal and low-iron diets.

(B) Representative H&E staining of spleens from WT and *Irp1*$^{-/-}$ mice on normal (N) or low-iron (L) diets showed increased red pulp and diminished white pulp (WP) in *Irp1*$^{-/-}$ mice.

(C) Spleens of 1-year-old mice of iron-starved *Irp1*$^{-/-}$ mice were significantly larger than in WT mice, demonstrating splenomegaly in *Irp1*$^{-/-}$ animals maintained on the low-iron diet.

(legend continued on next page)

observed (data not shown). Notably, the low-iron diet did not induce pulmonary hypertension or cardiac hypertrophy of the WT mice. Moreover, the resistance and tissue damping of *Irp1*$^{-/-}$ lung measured by FlexiVent were significantly lower (Figure S3D), and the oxygen and carbon dioxide tensions in arterial blood of *Irp1*$^{-/-}$ were normal (results not shown), suggesting that the pulmonary functions of *Irp1*$^{-/-}$ mice are within the normal range.

Pulmonary Hypertension in *Irp1*$^{-/-}$ Mice Was Associated with High Expression of HIF2α in Pulmonary Endothelial Cells and Transcriptional Activation of Endothelin-1

As abnormally high HIF2α expression has been implicated in the pathogenesis of polycythemia (Formenti et al., 2010) and pulmonary hypertension (Hickey et al., 2010), we evaluated the expression of HIF2α in the pulmonary vascular system. Although immunohistochemistry and immunoblots of total lung lysates did not reveal reproducible increases in HIF2α protein levels (data not shown), we found increased HIF2α expression in specific cells of other tissues such as kidney (Figure 2G) and spleen (Figure S4A). Moreover, in primary pulmonary endothelial cells isolated from WT and *Irp1*$^{-/-}$ animals, and cultured at low oxygen tensions, HIF2α protein levels increased significantly in *Irp1*$^{-/-}$ cells (Figure 4A) cultured under both normal and low-iron conditions, whereas mRNA levels did not increase (Figure S4B). Endothelin-1, a HIF target and potent vasoconstrictor, has been implicated in the pathogenesis of pulmonary hypertension, tissue hypertrophy, and fibrosis (Shao et al., 2011). We found that endothelin-1 expression significantly increased in *Irp1*$^{-/-}$ pulmonary endothelial cell lysates and cell media (Figure 4B, Figure S4C) but did not increase upon treatment with the iron chelator, desferrioxamine (Dfo). Endothelin-1 also increased in serum (Figure S4D) and lung tissue of *Irp1*$^{-/-}$ mice at 3 months of age, as determined by ELISA (Figure 4C) and mRNA quantification (Figure 4D), and also at 12 months of age (Figure S4E). As observed in primary pulmonary endothelial cells (Figure 4B), endothelin-1 expression did not increase in the lung tissue lysates of low-iron-diet *Irp1*$^{-/-}$ animals (Figure 4E), possibly explaining why pulmonary hypertension was not exacerbated by the low-iron diet. Expression of other known HIF targets also increased (Figures S4F–S4I), including Aldoa, a key glycolytic enzyme; Cxcl12, a chemokine involved in inflammation; Bnip3, a proapoptotic factor; and Retnla, also known as Himf (hypoxia-induced mitogenic factor), a member of the resistin family proposed to drive vascular remodeling and pulmonary hypertension in a mouse model of hypoxia-driven pulmonary hypertension (Hickey et al., 2010). In contrast, HIF1α protein levels did not change in *Irp1*$^{-/-}$ pulmonary endothelial cells (Figure 4A), indicating that the major prolyl hydroxylase-dependent HIF degradation pathway was not altered in *Irp1*$^{-/-}$ endothelial cells (Kaelin and Ratcliffe, 2008). Therefore, changes in HIF2α expression occurred in the absence of transcriptional changes or changes in degradation, implying that the loss of translational repressor activity caused by loss of *Irp1* was the major factor that drove increased HIF2α expression.

Differences in Tissue-Specific Expression Levels of Irp1 and Irp2 Explain Why *Irp1*$^{-/-}$ Mice Develop Polycythemia and Pulmonary Hypertension, whereas *Irp2*$^{-/-}$ Mice Develop Neurodegeneration

The two major phenotypic features of *Irp1*$^{-/-}$ animals reported here, namely polycythemia exacerbated by iron deficiency and associated with abdominal hemorrhage, and pulmonary hypertension associated with cardiac fibrosis, occurred respectively in two tissues, kidney and lung, that contained cells in which HIF2α expression increased markedly as a result of loss of Irp1 translational repressor activity. Notably, these phenotypes were not observed in *Irp2*$^{-/-}$ animals (data not shown). To explore why *Irp2*$^{-/-}$ mice lacked these phenotypes, we tested whether either Irp1 or Irp2 contributed to regulation of HIF2α expression in *Irp2*$^{-/-}$ or *Irp1*$^{-/-}$ mouse embryonic fibroblast (MEF) cells (Figure 5A), and we concluded from our results that both Irp1 and Irp2 can contribute to regulation of HIF2α expression. Then we compared relative contributions of Irp1 and Irp2 to total IRE-binding activity in several different tissues and cell lines. Notably, there was very little contribution from Irp2 in kidney or lung tissue (Figure 5B), whereas there was considerable contribution from Irp2 in brain, as previously reported (Meyron-Holtz et al., 2004a; Meyron-Holtz et al., 2004b). In *Irp1*$^{-/-}$ pulmonary endothelial cells, there was almost no detectable IRE binding activity (Figure 5C), even when cells were iron deprived, whereas Irp2 binding activity was readily detected in *Irp1*$^{-/-}$ embryonic fibroblasts (MEFs). These findings indicated that pulmonary endothelial cells depend almost exclusively on Irp1 to regulate the translation or stability of IRE-containing transcripts.

DISCUSSION

The polycythemia and systemic iron deficiency that developed in *Irp1*$^{-/-}$ mice reveal that Irp1 plays a pivotal role in balancing erythropoiesis and systemic iron homeostasis. As the master regulator of EPO expression, HIF2α was previously known to be regulated by hypoxia, anemia, and iron status through PHD2/vHL-mediated degradation (Gale et al., 2008; Smith et al., 2008; Bond et al., 2011). Here, we established that Irp1-mediated translational control plays a previously unrecognized critical role in regulation of HIF2α expression, and loss of Irp1 activity has serious physiological consequences.

Under hypoxic, anemic, and iron-deficient conditions, HIF2α protein stabilization induces EPO expression, which increases production of RBCs in a process that consumes large amounts of iron. When erythropoiesis consumes enough iron to cause nonerythroid tissue iron deficiency, synthesis of the iron sulfur

(D) Representative flow cytometric analyses of splenic cell populations from WT and *Irp1*$^{-/-}$ mice separated with antibodies to CD71 and Ter119 showed increase of Ter119+ erythroid precursors in *Irp1*$^{-/-}$ mice.
(E) Serum EPO levels measured by ELISA were increased in *Irp1*$^{-/-}$ mice, particularly in those on the low iron diet (n = 5–7 per group).
(F) Immunoblot analysis of nuclear fractions from kidney lysates (n = 5 per group) and (G) renal immunohistochemistry showed increased HIF2α protein expression in *Irp1*$^{-/-}$ mice that increased on the low-iron diets. Arrows point to interstitial fibroblasts in which intense dark purple stain indicates increased HIF2α expression. Data are represented as mean ± SD. See also Figure S2.

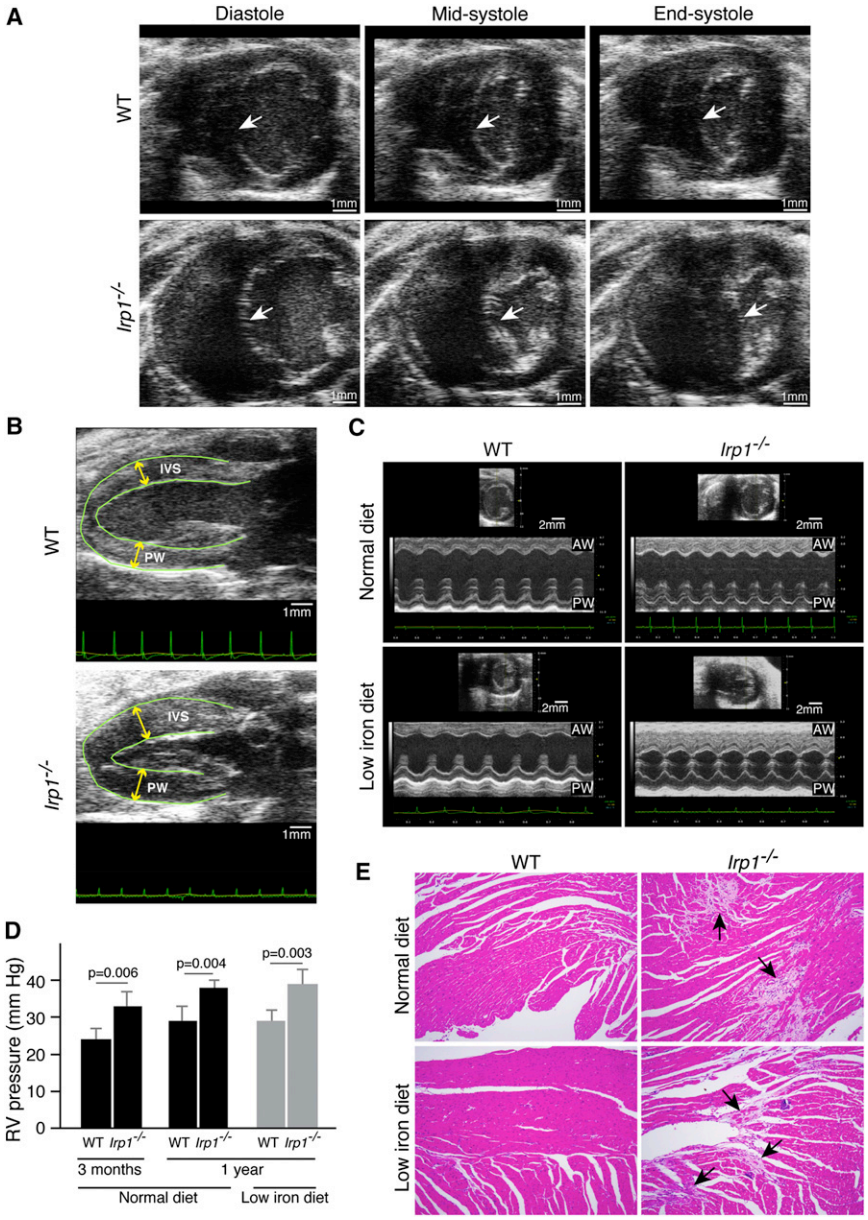

Figure 3. *Irp1*$^{-/-}$ Mice Developed Pulmonary Hypertension and Cardiac Fibrosis

(A) Representative cardiac ultrasound images showed abnormal motion of the interventricular septum (IVS) (arrows) during the cardiac cycle. The IVS flattened and was pushed inward into the left ventricle (LV) chamber at the end of systole, giving the LV a D-shaped appearance in the low-iron-diet *Irp1*$^{-/-}$ mice, suggesting that right ventricular (RV) pressure was high, whereas the IVS maintained a normal concave shape throughout systole in the WT mice on low-iron diets (n = 5 per group).

(B) In representative parasternal long axis views of the left ventricle, the IVS and posterior walls (PW) of the left ventricle were hypertrophied in the iron-starved *Irp1*$^{-/-}$ mice compared with the iron-starved wild-type mice (n = 5 per group).

(C) Representative parasternal short axis M mode of the left ventricle demonstrated significant hypertrophy of the anterior (AW) and posterior walls (PW) in *Irp1*$^{-/-}$ mice on low-iron diets (n = 5 per group).

(D) Right ventricular (RV) pressure measured by catheterization of lightly anesthetized 3-month and 1-year-old WT and *Irp1*$^{-/-}$ mice showed significantly elevated pressures in *Irp1*$^{-/-}$ mice. Data are represented as mean ± SD (n = 3 per group).

(E) Representative H&E staining of hearts from WT and *Irp1*$^{-/-}$ mice on normal and low-iron diet showed extensive fibrosis in *Irp1*$^{-/-}$ mice, though cardiac function was not compromised (see text). See also Figure S3, Movie S1.

cluster of Irp1 is decreased, and Irp1 converts to the apoprotein form that binds to IREs. Apo-Irp1 represses HIF2α translation, decreases EPO production, and thereby diminishes RBC production (Figure 6). Through this Irp1/HIF2α-dependent feedback mechanism, the body balances erythropoietic activity and systemic iron availability to ensure that high RBC production in iron-deficient animals does not deplete iron stores in tissues such as the heart, brain, and kidneys and compromise crucial cellular functions such as mitochondrial respiration. In *Irp1*$^{-/-}$ mice, derepression of HIF2α translation increases HIF2α protein levels, which stimulates EPO expression, which in turn drives red cell production and concomitant systemic iron deficiency. Moreover, iron deficiency can further stabilize HIF2α protein levels by diminishing activity of the iron-dependent prolyl hydroxylases involved in its degradation and can thereby exacerbate the polycythemia further (Percy et al., 2006; Kaelin and Ratcliffe, 2008). An increase in the total red cell volume can increase the blood viscosity and resistance in vascular tissues, and can thereby endanger the cardiovascular system. As shown in the model in Figure 6, we propose that the extremely high hematocrits of *Irp1*$^{-/-}$ mice on a low-iron diet contribute to sudden death from abdominal hemorrhages, perhaps because the high viscosity leads to localized blood pressure increases. Thus, *Irp1*$^{-/-}$ mice represent a unique model in which iron deficiency exacerbates a mild polycythemia rather than causing anemia, and in which iron supplementation partially reverses the polycythemia. *Irp1*$^{-/-}$ mice reveal that the anemia of iron deficiency normally results from a restriction of EPO production mediated by renal Irp1, which represses HIF2α translation and EPO expression when the kidney is iron deficient.

Irp1$^{-/-}$ mice develop pulmonary hypertension, and pulmonary endothelial cells represent another tissue in which Irp1 appears to play a dominant role. Since the pulmonary endothelial cells represent a small fraction of the total population of cells in the lung tissue and they form a thin cell layer covering the vascular lumen, we did not consistently detect increased HIF2α

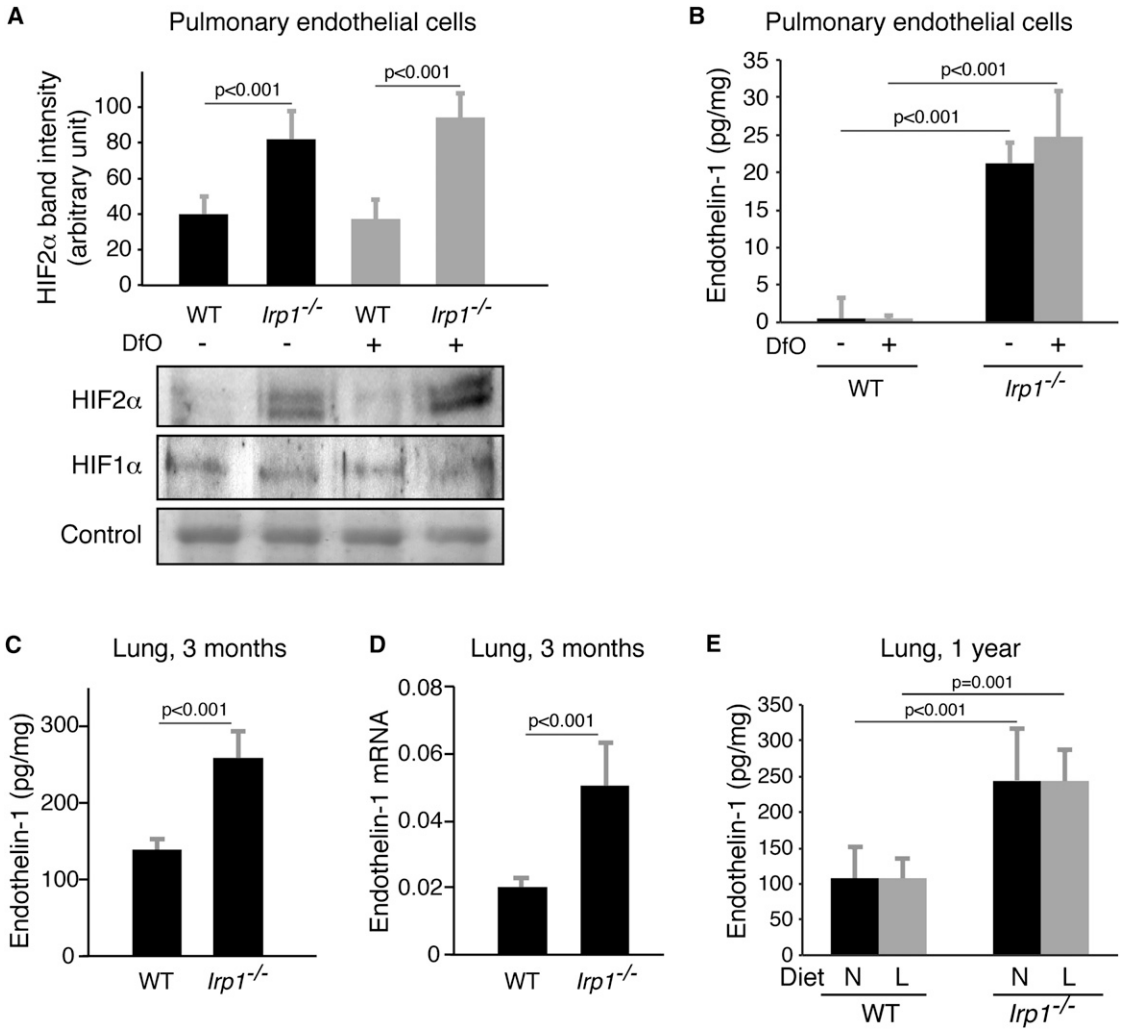

Figure 4. Pulmonary Hypertension in *Irp1*$^{-/-}$ Mice Was Associated with High Expression of HIF2α in Pulmonary Endothelial Cells and Transcriptional Activation of Multiple Targets

(A) HIF2α protein expression increased in the nuclear fractions of *Irp1*$^{-/-}$ pulmonary endothelial cells relative to WT pulmonary endothelial cells isolated from mice, cultured at 1% oxygen, and treated (for 15 hr) with or without the iron chelator, desferrioxamine (Dfo,100 μM), whereas HIF1α protein levels remained unchanged.

(B) Endothelin-1 levels (measured by ELISA) in the lysates of pulmonary endothelial cells isolated from WT and *Irp1*$^{-/-}$ mice and cultured at 1% oxygen (n = 6 per group).

(C) Endothelin-1 levels in lung lysates of 3-month-old normal diet mice measured by ELISA (n = 5–6 per group).

(D) Endothelin-1 mRNA levels in lungs of 3-month-old normal-diet mice.

(E) Endothelin-1 levels in lung lysates of 1-year-old normal and low-iron-diet mice measured by ELISA (n = 5 per group). Data are represented as mean ± SD. See also Figure S4.

expression in western blots or immunohistochemistry. However, we cultured primary pulmonary endothelial cells and found that HIF2α was significantly increased in primary pulmonary endothelial cells from *Irp1*$^{-/-}$ mice. Increased HIF2α expression was also confirmed by the expression of some well-known HIFα targets including the potent vasoconstrictor, endothelin-1. Endothelin-1 expression is significantly increased in *Irp1*$^{-/-}$ mice and likely plays a major role in the pathogenesis of pulmonary hypertension. Endothelin-1 is known to bind to endothelin-1 receptor type A (ETAR) on smooth muscle cells in the vascular wall and to induce the contraction of blood vessels (Shao et al., 2011), leading to increased pulmonary hypertension, as we observed. Endothelin-1 also binds to ETAR on cardiomyocytes and fibroblasts and induces their proliferation, leading to cardiac hypertrophy and fibrosis (Thorin and Clozel, 2010). The pulmonary hypertension may also contribute to the cardiac hypertrophy by increasing the workload of the heart as it works against high resistance in the pulmonary vasculature. The spontaneous pulmonary hypertension of *Irp1*$^{-/-}$ mice warrants further investigation.

An important role for HIF2α in development of polycythemia and pulmonary hypertension was recently reported in a mouse model of Chuvash polycythemia (Hickey et al., 2007, 2010). In Chuvash polycythemia patients, the vHL^{R200W} mutation leads

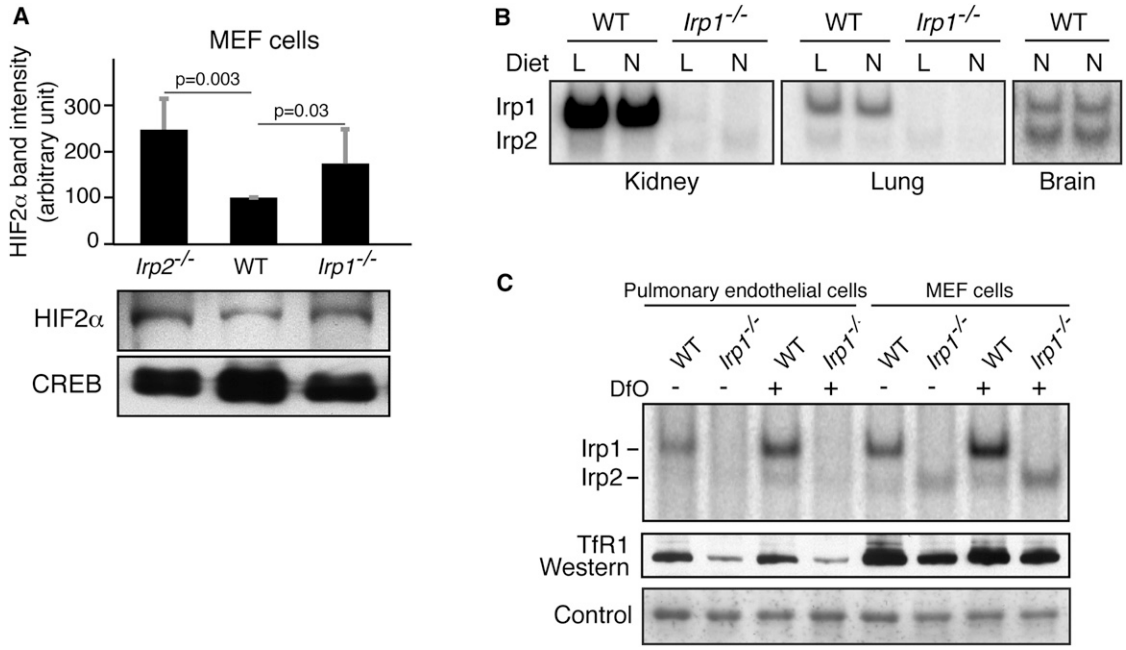

Figure 5. Irp1 Is the Major Contributor of IRE-Binding Activity in Kidney and Lung Tissues and in Pulmonary Endothelial Cells

(A) HIF2α western with nuclear fractions of *Irp2*$^{-/-}$, WT, and *Irp1*$^{-/-}$ MEF cells showed that HIF2α expression increased equally upon loss of either Irp1 or Irp2. Data (n = 5 per group) are represented as mean ± SD.

(B) IRE-binding activity assays of kidney, lung, and forebrain lysates of normal-diet (N) and low-iron-diet (L) WT and *Irp1*$^{-/-}$ mice showed that most of the IRE-binding activity in kidney and lung tissues was contributed by Irp1, whereas Irp1 was not the major contributor of IRE-binding activity in brain.

(C) IRE binding activity and TfR1 western blots of WT and *Irp1*$^{-/-}$ mouse pulmonary endothelial cell lysates and MEF cell lysates in the absence and presence of 100 μM Dfo showed that there was very little contribution from Irp2 to the total IRE-binding activity in pulmonary endothelial cells both at normal and low-iron conditions (left lanes), whereas Irp2 was readily detectable in MEFs (right lanes).

to highly expressed HIF2α protein, which stimulates EPO production and polycythemia, and also promotes increased endothelin-1 expression and pulmonary hypertension in the lungs (Sable et al., 2012). In a Chuvash mouse model carrying the identical mutation as human patients, mice were protected from developing pulmonary hypertension by heterozygous deletion of HIF2α, whereas HIF1α deletion did not prevent pulmonary hypertension and vascular remodeling, supporting the idea that HIF2α was pivotal in the pathophysiology of polycythemia and pulmonary hypertension in the mouse model, and by inference, in the Chuvash patients. As in *Irp1*$^{-/-}$ mice, Chuvash patients also show decreased serum iron levels and transferrin saturation, supporting the notion that iron redistributes into RBC production. The HIF2α heterozygous mice were also previously shown to have resistance to pulmonary hypertension caused by chronic hypoxia, supporting the essential role of HIF2α in this process (Brusselmans et al., 2003). Moreover, the HIF2α locus was recently implicated as being important in successful adaptation to chronic hypoxia at high altitude (Bigham et al., 2010; Yi et al., 2010). *Irp1*$^{-/-}$ mice confirm the central role of HIF2α in regulating erythropoiesis and pulmonary hypertension, emphasize the importance of Irp1 in controlling HIF2α expression, and also suggest a potential treatment for HIF2α-related diseases including Chuvash polycythemia. Pharmaceutical activation of the IRE binding activity of Irp1 by chemicals such as Tempol (Ghosh et al., 2008) or nitric oxide could potentially repress HIF2α translation and alleviate the polycythemia and pulmonary hypertension in patients with problems in the Irp/HIF2α axis.

In conclusion, our results in *Irp1*$^{-/-}$ mice show that Irp1 plays an important function in regulating erythropoiesis and maintaining balance with systemic iron status, and the regulation of Irp1 on HIF2α translation represents an important aspect of fine-tuning of HIF2α expression in physiology. Since human genomes were recently shown to contain at least 20 loss-of-function mutations per genome (MacArthur et al., 2012), and *Irp1*$^{-/-}$ mice survive to adulthood, we suggest that loss-of-function mutations of Irp1 may underlie previously unexplained pulmonary hypertension and/or polycythemia in some patients.

EXPERIMENTAL PROCEDURES

Mice

Irp1$^{-/-}$ animals were generated by targeting Aco1 (Irp1), propagated by breeding, and genotyped by Southern blotting using gene-specific probes as previously described (Meyron-Holtz et al., 2004a). WT and *Irp1*$^{-/-}$ mice used in this study have a mixed genetic background consisting of 129S4/SvJae and C57Bl/6. The mice were weaned 3–4 weeks after their birth. Immediately after weaning, mice were maintained on a diet either containing 3.7 ± 0.9 (measured by ICP-MS) mg iron/kg chow (low-iron diet) from Harlan Teklad or normal diet containing 143 ± 18 mg iron/kg (measured by ICP-MS) chow (normal diet). Experiments with blood and tissues were performed with 1-year-old mice unless otherwise noted. Whenever possible, siblings were used in matched study sets to minimize phenotypic variation due to genetic background. Mice of different genotypes and diets were age and gender matched for statistical comparisons. All the mouse experiments were done

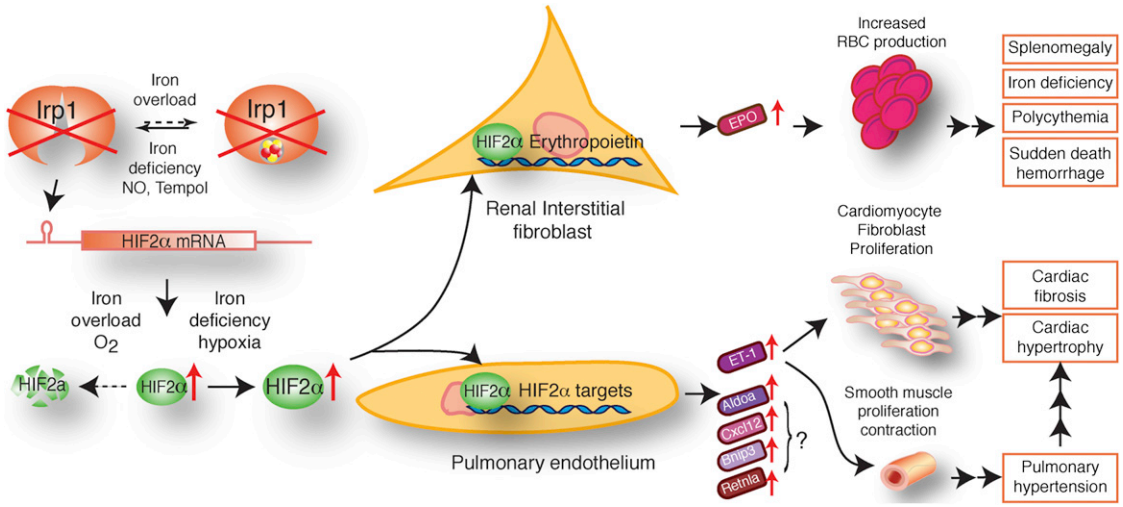

Figure 6. Model for the Molecular Pathogenesis of Polycythemia and Pulmonary Hypertension in *Irp1*$^{-/-}$ Mice

In renal interstitial fibroblasts and pulmonary endothelial cells, where Irp1 is the predominant IRE-binding protein, Irp1 deficiency results in increased HIF2α expression through derepression of HIF2α translation. In renal interstitial fibroblasts, HIF2α induces high expression of EPO, which promotes increased RBC production and consumption of high amounts of iron, thereby causing iron deficiency in nonerythroid tissues. Importantly, the tissue iron deficiency can stabilize HIF2α protein further and exacerbate the polycythemia. The systemic iron deficiency and high hematocrits probably stress the cardiovascular system and lead to sudden death from hemorrhages. In pulmonary endothelial cells, elevated expression of HIF2α leads to increased endothelin-1 (ET-1) expression. By binding to ETAR, ET-1 induces the proliferation and contraction of vascular smooth muscle cells, resulting in pulmonary hypertension. ET-1 also induces cardiac fibrosis and hypertrophy when it binds to ETAR. HIF2α also drives increased expression of other HIFα targets, including Aldoa, Cxcl12, Bnip3, and Retnla, and their potential contributions to pulmonary hypertension remain to be investigated in *Irp1*$^{-/-}$ mice.

following protocols approved by the NICHD Animal Care and Use Committee and met NIH guidelines for the humane care of animals.

Hematocrit Measurements

Approximately 100 μl of blood was harvested in to a heparin-coated tube (BD microtainer tubes with lithium heparin) from each mouse by mandibular method. Hematocrit tubes were filled with blood to three-quarters full by capillary action, sealed, and centrifuged for 5 min in a microhematocrit centrifuge (LW Scientific). The hematocrit was measured with the help of a hematocrit reader.

CBC Measurement

Blood was drawn from mice by mandibular method or by cardiac puncture in deeply anesthetized mice prior to euthanizing. CBCs were performed on a Hemavet 1500 (Drew Scientific, Dallas, Texas) analyzer.

Intracardial Pressure Measurements

Intraventricular pressures were measured invasively by using a microtip pressure transducer catheter connected to an electrostatic chart recorder (Millar Instruments, Houston). The mice were anesthetized with 1%–3% isoflurane, and the right external jugular veins were cannulated. For each mouse, the catheter was advanced to the right ventricle. Correct placement was verified according to RV pressure curve, and the pressure and volume tracings were recorded. Body temperature of the mice was maintained between 37°C and 38°C, and the data were recorded using LabChart software (AD Instruments, Colorado Springs). This was a nonsurvival procedure. Animals were euthanized, while under anesthesia, by cervical dislocation verified by thoracotomy, or by exsanguination under anesthesia verified by thoracotomy.

Echocardiography

Transthoracic echocardiography was performed with 1-year-old mice with a high-frequency ultrasound system (VisualSonics, Vevo 2100). All images were acquired using a MS-400 transducer (VisualSonics) with a center operating frequency of 30 MHz, and broadband frequency of 18–38 MHz. The axial resolution of this transducer is 50 μm, and the footprint is 20 mm × 5 mm. 2D images were obtained for multiple views of the heart. M mode images of the left ventricle were collected from the parasternal short axis view at the level of the midpapillary muscles and obtained by rotating the probe 90° clockwise from the parasternal long axis view. From the M mode images the LV systolic and diastolic posterior and anterior wall thicknesses, as well as end systolic and end diastolic internal LV chamber dimensions (LVIDs, LVIDd), were measured using the leading edge method. The LV functional value of ejection fraction (EF) was calculated from chamber dimension measurements through system software as follows: %EF = 100 ((LV vol;d − LV vol;s)/LV Vol;d) where LV vol;d = ((7.0/(2.4 + LVID;d)) × LVID;d^3 and LV Vol;s = ((7.0/(2.4 × LVID;s)) × LVID;s^3.

Flexivent Procedure for Measurement of Pulmonary Function

To measure lung mechanics, mice were anesthetized, and a cannula was inserted into the trachea. The mice were then attached to the Scireq FlexiVent system and were mechanically ventilated. The maintenance of tidal volume and respiration rate were controlled (150–200 bpm, 7–9 ml/kg, PEEP 3 cm H20). A few brief sighs were given to the mouse to determine lung volume information but did not exceed 25 cm H_20. After that, the mice were euthanized while under anesthesia.

Pulmonary Vessel Thickness Assessment

Quantification of the pulmonary vascular media and intima thickness was performed as previously described (Graham et al., 2010).

Immunohistochemistry

Staining for HIF2α was performed following previously published (Jeong and David, 2006) protocol using rabbit anti-HIF2α antibody (IHC World). Sections were analyzed using a bright-field microscope (Nikon Eclipse E600).

Fluorescence-Activated Cell Sorting

Freshly isolated spleens were gently poked in cold PBS with forceps to release the cells, and the cell suspensions were filtered with a cell strainer to generate single-cell suspensions. The cells were washed in PBS and resuspended in PBA buffer (1% bovine serum albumin, 0.1% sodium azide in PBS [pH 7.4]). Cells (1 × 10^6) were incubated with FITC-labeled rat anti-mouse CD71 and PE-CY7 labeled rat anti-mouse TER119 antibodies (BD PharMingen) in PBA buffer at 4°C for 30 min and then were analyzed by FACS on BD FACS Calibur.

Erythropoietin and Endothelin-1 Measurement by ELISA

EPO and endothelin-1 were measured by ELISA kit (R&D Systems) according to the manufacturer's protocol. The lung lysates were prepared in RIPA buffer (50 mM Tris, 150 mM NaCl, 0.1% SDS, 0.5% Na.deoxycholate, 1% Triton X-100) and diluted 100 times before being measured by ELISA.

Measurement of Total Serum Iron and Transferrin Saturation

Serum iron and unsaturated iron-binding capacity (UIBC) were measured in nonhemolyzed mouse serum using a Pointe Scientific (Lincoln Park, MI) Iron/TIBC Reagent Set following the manufacturer's instructions. Transferrin saturation was calculated from measured serum iron and UIBC.

Measurement of Iron Concentration in Spleen

Animals were deeply anesthetized, and blood was removed by extensively perfusing PBS through the hearts. Spleens were harvested and immediately snap frozen in liquid nitrogen. Total iron concentrations were measured by inductively coupled plasma mass spectroscopy (ICP-MS) as described (Kim et al., 2009).

Cell Culture

For pulmonary endothelial cells, endothelial cells from lungs of WT and *Irp1*$^{-/-}$ mice were isolated following the method of Sobczak et al. (Sobczak et al., 2010). Lungs from three 8-day-old WT and *Irp1*$^{-/-}$ pups were used for isolation of pulmonary endothelial cells. The cells were grown at 1% oxygen and harvested for experiments when they became about 80% confluent. MEFs of 13-day-old embryos were isolated and cultured from WT, *Irp1*$^{-/-}$, and *Irp2*$^{-/-}$ mice as previously described (Meyron-Holtz et al., 2004a, 2004b).

RNA Mobility-Shift Assays

Gel retardation assays were performed as previously described (Meyron-Holtz et al., 2004a) with lysate containing 10 μg of total protein.

Western Blotting and Antibodies

Protein analysis was carried out as previously described (LaVaute et al., 2001). HIF1α and HIF2α westerns were performed with nuclear fractions separated following the protocol of "Active Motif" (http://www.activemotif.com/) from tissues and cells. HIF2α antibody (affinity-purified goat anti-human) was from R&D Systems, and a final concentration of 1.0 μg/ml was used as described in R&D protocol. Purified mouse anti-human HIF1α antibody from BD Biosciences was used at 1:1,000 dilution. A mouse monoclonal Tfr1 antibody from Zymed was used at 1:2,000 dilution. Western blots were treated with secondary peroxidase-conjugated bovine anti-goat IgG antibody from Santa Cruz Biotechnology, Inc. or sheep anti-mouse IgG antibody from GE Healthcare at 1:1,000 and 1:2,000 dilutions, respectively. HIF1α and HIF2α western blots were developed using supersignal west femto maximum sensitivity substrate (Thermoscientific). All other western blots were developed using supersignal west pico chemiluminescent substrate (Thermoscientific).

Quantitative Real-Time PCR

Total RNA was prepared with TRIzol reagent (Invitrogen), cDNA was prepared with High Capacity cDNA Reverse Transcription kit (Applied Biosystems) with 2 μg total RNA. Quantitative real-time PCR (qRT-PCR) experiments were performed with SYBR Green PCR master mixture (Applied Biosystems). The primers for DMT1, FPN1, Dcytb, hepcidin, endothelin-1, EPO, HIF1alpha, HIF2alpha, ALDOA, CCXL12, Bnip3, Retnla, and actin are shown in Table S1. The results were normalized against actin levels.

Statistical Analyses

Where applicable, data are expressed as the mean ± standard deviation. Pairwise comparisons between two groups were analyzed using the unpaired Student's t test. Analyses of multiple groups were performed using two-way ANOVA. p values of less than 0.05 were considered statistically significant. For statistical analysis of mouse survival time, survival curves were plotted using the Kaplan-Meier method and evaluated by log-rank test using the XLSTAT software package from Addinsoft.

SUPPLEMENTAL INFORMATION

Supplemental Information includes four figures, two tables, one movie, and Supplemental Experimental Procedures and can be found with this article at http://dx.doi.org/10.1016/j.cmet.2012.12.016.

ACKNOWLEDGMENTS

This work was supported by the intramural programs of NICHD and NHLBI. We thank Gregory Holmes-Hampton for helpful discussions, Michele Allen for her help in mouse studies, Shawn Kozlov for blood gas measurements, and Javier Seravalli for performing metal measurements. R.M.T.'s research was supported by NIH (RC1HL100849). M.C.G. and D.-L.Z. designed the study, generated data, performed analyses, and wrote the paper. S.Y.J. and D.A.S. generated data, performed analyses, and wrote the paper. G.K., A.N., D.R.C., B.B.G., Z.-X.Y., M.E., and J.L. generated data and performed analyses. H.O.-W., T.T., T.S., G.R., K.R., and A.S. generated data. W.-H.T. and R.M.T. provided substantial intellectual contribution. T.A.R. designed the study, performed analyses, and wrote the paper.

Received: July 23, 2012
Revised: October 12, 2012
Accepted: December 31, 2012
Published: February 5, 2013

REFERENCES

Bigham, A., Bauchet, M., Pinto, D., Mao, X., Akey, J.M., Mei, R., Scherer, S.W., Julian, C.G., Wilson, M.J., López Herráez, D., et al. (2010). Identifying signatures of natural selection in Tibetan and Andean populations using dense genome scan data. PLoS Genet. *6*, e1001116. http://dx.doi.org/10.1371/journal.pgen.1001116.

Bond, J., Gale, D.P., Connor, T., Adams, S., de Boer, J., Gascoyne, D.M., Williams, O., Maxwell, P.H., and Ancliff, P.J. (2011). Dysregulation of the HIF pathway due to VHL mutation causing severe erythrocytosis and pulmonary arterial hypertension. Blood *117*, 3699–3701.

Brusselmans, K., Compernolle, V., Tjwa, M., Wiesener, M.S., Maxwell, P.H., Collen, D., and Carmeliet, P. (2003). Heterozygous deficiency of hypoxia-inducible factor-2alpha protects mice against pulmonary hypertension and right ventricular dysfunction during prolonged hypoxia. J. Clin. Invest. *111*, 1519–1527.

Cooperman, S.S., Meyron-Holtz, E.G., Olivierre-Wilson, H., Ghosh, M.C., McConnell, J.P., and Rouault, T.A. (2005). Microcytic anemia, erythropoietic protoporphyria, and neurodegeneration in mice with targeted deletion of iron-regulatory protein 2. Blood *106*, 1084–1091.

Dupuy, J., Volbeda, A., Carpentier, P., Darnault, C., Moulis, J.M., and Fontecilla-Camps, J.C. (2006). Crystal structure of human iron regulatory protein 1 as cytosolic aconitase. Structure *14*, 129–139.

Formenti, F., Constantin-Teodosiu, D., Emmanuel, Y., Cheeseman, J., Dorrington, K.L., Edwards, L.M., Humphreys, S.M., Lappin, T.R., McMullin, M.F., McNamara, C.J., et al. (2010). Regulation of human metabolism by hypoxia-inducible factor. Proc. Natl. Acad. Sci. USA *107*, 12722–12727.

Gale, D.P., Harten, S.K., Reid, C.D., Tuddenham, E.G., and Maxwell, P.H. (2008). Autosomal dominant erythrocytosis and pulmonary arterial hypertension associated with an activating HIF2 alpha mutation. Blood *112*, 919–921.

Galy, B., Ferring, D., Minana, B., Bell, O., Janser, H.G., Muckenthaler, M., Schümann, K., and Hentze, M.W. (2005). Altered body iron distribution and microcytosis in mice deficient in iron regulatory protein 2 (IRP2). Blood *106*, 2580–2589.

Ghosh, M.C., Tong, W.H., Zhang, D., Ollivierre-Wilson, H., Singh, A., Krishna, M.C., Mitchell, J.B., and Rouault, T.A. (2008). Tempol-mediated activation of latent iron regulatory protein activity prevents symptoms of neurodegenerative disease in IRP2 knockout mice. Proc. Natl. Acad. Sci. USA *105*, 12028–12033.

Graham, B.B., Mentink-Kane, M.M., El-Haddad, H., Purnell, S., Zhang, L., Zaiman, A., Redente, E.F., Riches, D.W., Hassoun, P.M., Bandeira, A., et al.

(2010). Schistosomiasis-induced experimental pulmonary hypertension: role of interleukin-13 signaling. Am. J. Pathol. *177*, 1549–1561.

Hentze, M.W., Muckenthaler, M.U., Galy, B., and Camaschella, C. (2010). Two to tango: regulation of Mammalian iron metabolism. Cell *142*, 24–38.

Hickey, M.M., Lam, J.C., Bezman, N.A., Rathmell, W.K., and Simon, M.C. (2007). von Hippel-Lindau mutation in mice recapitulates Chuvash polycythemia via hypoxia-inducible factor-2 alpha signaling and splenic erythropoiesis. J. Clin. Invest. *117*, 3879–3889.

Hickey, M.M., Richardson, T., Wang, T., Mosqueira, M., Arguiri, E., Yu, H., Yu, Q.C., Solomides, C.C., Morrisey, E.E., Khurana, T.S., et al. (2010). The von Hippel-Lindau Chuvash mutation promotes pulmonary hypertension and fibrosis in mice. J. Clin. Invest. *120*, 827–839.

Jeong, S.Y., and David, S. (2006). Age-related changes in iron homeostasis and cell death in the cerebellum of ceruloplasmin-deficient mice. J. Neurosci. *26*, 9810–9819.

Kaelin, W.G., Jr., and Ratcliffe, P.J. (2008). Oxygen sensing by metazoans: the central role of the HIF hydroxylase pathway. Mol. Cell *30*, 393–402.

Kim, H., Son, H.Y., Bailey, S.M., and Lee, J. (2009). Deletion of hepatic Ctr1 reveals its function in copper acquisition and compensatory mechanisms for copper homeostasis. Am. J. Physiol. Gastrointest. Liver Physiol. *296*, G356–G364.

LaVaute, T., Smith, S., Cooperman, S., Iwai, K., Land, W., Meyron-Holtz, E., Drake, S.K., Miller, G., Abu-Asab, M., Tsokos, M., et al. (2001). Targeted deletion of the gene encoding iron regulatory protein-2 causes misregulation of iron metabolism and neurodegenerative disease in mice. Nat. Genet. *27*, 209–214.

MacArthur, D.G., Balasubramanian, S., Frankish, A., Huang, N., Morris, J., Walter, K., Jostins, L., Habegger, L., Pickrell, J.K., Montgomery, S.B., et al.; 1000 Genomes Project Consortium. (2012). A systematic survey of loss-of-function variants in human protein-coding genes. Science *335*, 823–828.

Majmundar, A.J., Wong, W.J., and Simon, M.C. (2010). Hypoxia-inducible factors and the response to hypoxic stress. Mol. Cell *40*, 294–309.

Meyron-Holtz, E.G., Ghosh, M.C., Iwai, K., LaVaute, T., Brazzolotto, X., Berger, U.V., Land, W., Ollivierre-Wilson, H., Grinberg, A., Love, P., and Rouault, T.A. (2004a). Genetic ablations of iron regulatory proteins 1 and 2 reveal why iron regulatory protein 2 dominates iron homeostasis. EMBO J. *23*, 386–395.

Meyron-Holtz, E.G., Ghosh, M.C., and Rouault, T.A. (2004b). Mammalian tissue oxygen levels modulate iron-regulatory protein activities in vivo. Science *306*, 2087–2090.

Pan, X., Suzuki, N., Hirano, I., Yamazaki, S., Minegishi, N., and Yamamoto, M. (2011). Isolation and characterization of renal erythropoietin-producing cells from genetically produced anemia mice. PLoS ONE *6*, e25839. http://dx.doi.org/10.1371/journal.pone.0025839.

Percy, M.J., Zhao, Q., Flores, A., Harrison, C., Lappin, T.R., Maxwell, P.H., McMullin, M.F., and Lee, F.S. (2006). A family with erythrocytosis establishes a role for prolyl hydroxylase domain protein 2 in oxygen homeostasis. Proc. Natl. Acad. Sci. USA *103*, 654–659.

Rouault, T.A. (2006). The role of iron regulatory proteins in mammalian iron homeostasis and disease. Nat. Chem. Biol. *2*, 406–414.

Sable, C.A., Aliyu, Z.Y., Dham, N., Nouraie, M., Sachdev, V., Sidenko, S., Miasnikova, G.Y., Polyakova, L.A., Sergueeva, A.I., Okhotin, D.J., et al. (2012). Pulmonary artery pressure and iron deficiency in patients with upregulation of hypoxia sensing due to homozygous VHL(R200W) mutation (Chuvash polycythemia). Haematologica *97*, 193–200.

Salahudeen, A.A., Thompson, J.W., Ruiz, J.C., Ma, H.W., Kinch, L.N., Li, Q., Grishin, N.V., and Bruick, R.K. (2009). An E3 ligase possessing an iron-responsive hemerythrin domain is a regulator of iron homeostasis. Science *326*, 722–726.

Sanchez, M., Galy, B., Muckenthaler, M.U., and Hentze, M.W. (2007). Iron-regulatory proteins limit hypoxia-inducible factor-2alpha expression in iron deficiency. Nat. Struct. Mol. Biol. *14*, 420–426.

Semenza, G.L. (2012). Hypoxia-inducible factors in physiology and medicine. Cell *148*, 399–408.

Shao, D., Park, J.E., and Wort, S.J. (2011). The role of endothelin-1 in the pathogenesis of pulmonary arterial hypertension. Pharmacol. Res. *63*, 504–511.

Smith, S.R., Ghosh, M.C., Ollivierre-Wilson, H., Hang Tong, W., and Rouault, T.A. (2006). Complete loss of iron regulatory proteins 1 and 2 prevents viability of murine zygotes beyond the blastocyst stage of embryonic development. Blood Cells Mol. Dis. *36*, 283–287.

Smith, T.G., Brooks, J.T., Balanos, G.M., Lappin, T.R., Layton, D.M., Leedham, D.L., Liu, C., Maxwell, P.H., McMullin, M.F., McNamara, C.J., et al. (2008). Mutation of the von Hippel-Lindau gene alters human cardiopulmonary physiology. Adv. Exp. Med. Biol. *605*, 51–56.

Sobczak, M., Dargatz, J., and Chrzanowska-Wodnicka, M. (2010). Isolation and culture of pulmonary endothelial cells from neonatal mice. J. Vis. Exp. *46*, 2316. http://dx.doi.org/10.3791/2316.

Thorin, E., and Clozel, M. (2010). The cardiovascular physiology and pharmacology of endothelin-1. Adv. Pharmacol. *60*, 1–26.

Vashisht, A.A., Zumbrennen, K.B., Huang, X., Powers, D.N., Durazo, A., Sun, D., Bhaskaran, N., Persson, A., Uhlen, M., Sangfelt, O., et al. (2009). Control of iron homeostasis by an iron-regulated ubiquitin ligase. Science *326*, 718–721.

Walden, W.E., Selezneva, A.I., Dupuy, J., Volbeda, A., Fontecilla-Camps, J.C., Theil, E.C., and Volz, K. (2006). Structure of dual function iron regulatory protein 1 complexed with ferritin IRE-RNA. Science *314*, 1903–1908.

Yi, X., Liang, Y., Huerta-Sanchez, E., Jin, X., Cuo, Z.X., Pool, J.E., Xu, X., Jiang, H., Vinckenbosch, N., Korneliussen, T.S., et al. (2010). Sequencing of 50 human exomes reveals adaptation to high altitude. Science *329*, 75–78.

Zimmer, M., Ebert, B.L., Neil, C., Brenner, K., Papaioannou, I., Melas, A., Tolliday, N., Lamb, J., Pantopoulos, K., Golub, T., and Iliopoulos, O. (2008). Small-molecule inhibitors of HIF-2a translation link its 5'UTR iron-responsive element to oxygen sensing. Mol. Cell *32*, 838–848.